Authors Preprint Original version available at:
Submitted to: Laser Physics Letters https://doi.org/10.1088/1612-202X/ad9149

Refined Speckle Contrast Estimation in OCT based on Compensation of Scattering-Related Distortions of Speckle Pattern Parameters

Lev A. Matveev[1,2], Alexander A. Sovetsky[1], Alexander L. Matveyev[1], I. Alex Vitkin[3,4,5], Maher Assaad[2] and Vladimir Y. Zaitsev*[1]

[1]Russian Academy of Sciences, Uljanova St 46, Nizhny Novgorod, 603950, Russia
[2]Ajman University, Department of Electrical and Computer Engineering, Ajman 666688, United Arab Emirates
[3]University of Toronto, Department of Medical Biophysics, 101 College St., M5G 1 L7 Toronto, Canada
[4]University Health Network, Princess Margaret Cancer Centre, 101 College St., M5G 1 L7 Toronto, Canada
[5]University of Toronto, Department of Radiation Oncology, 101 College St., M5G 1 L7 Toronto, Canada

All requests related to the www.opticelastograph.com platform and tools, as well as those related to https://github.com/OCTDigitalPhantoms/LPL_SC_2024_data-DOI-10.1088-1612-202X-ad9149/, can be addressed to Dr. Lev Matveev.
Contact: drlevmatveev@gmail.com

Abstract

Speckle contrast (SC) parameter in optical coherence tomography (OCT) scans is formed by the interplay of several factors - local level of optical wave backscattering by the material inhomogeneities, parameters of spatial distribution of the latter and the degree of cumulative optical wave attenuation during its forth-and-back propagation. For the optical wavelengths used in OCT, this attenuation usually is dominated by the influence of scattering in the visualized turbid tissues rather than by absorption. For sufficiently high concentration of scatterers (at least a few scatterers in the coherence volume) characterized by comparable scattering strengths and fairly homogeneous distribution in space, the interference of locally scattered waves should be characterized by a Rayleigh distribution of speckle amplitudes, for which the local SC tends to 0.52. Equivalently, in terms of speckle intensities, the local SC tends to unity. Local spatial inhomogeneities or strongly uneven scattering strengths lead to appearance of increased values of SC, which may serve as a diagnostic feature of some tissue components in OCT images. At the same time, in comparison to surface speckles formed by coherent-light scattering from rough surfaces, OCT-beam attenuation during its forth-and-back propagation may introduce intensity inhomogeneities in OCT scans even for homogeneous tissue areas. This effect results in artefactual distortion of the visible SC in comparison with the above-mentioned expected value. Moreover, the presence of individual strong scatterers may additionally non-locally distort SC values due to appearance of elongated shadows below such scatterers, which causes lateral inhomogeneities in OCT scans. Here, we propose a refined SC parameter, which is cleaned from distorting scattering-related effects in both axial and lateral directions. Depth-resolved estimation of optical attenuation coefficient is used to restore attenuation-free OCT scans, for which the refined SC is estimated. The efficiency of the proposed approach is demonstrated using both digital OCT phantoms with highly controlled properties and experimental OCT data.

Keywords: optical coherence tomography, OCT speckles, optical attenuation coefficient, speckle contrast

1. Introduction

Optical Coherence Tomography (OCT) is a multimodal tool for biomedical imaging based on principles of low-coherence interferometry. It provides depth-resolved scans with a typical resolution of 3-10 μm and a visualization depth of 1-2 millimeters [1]. In comparison to other speckle-contrast techniques, in which planar speckle patterns arise due to diffuse scattering of coherent light from rough surfaces, speckles in OCT scans are formed by nearly ballistic backscattering of collimated beams. Therefore, OCT speckles are formed by the interference of backscattered

waves propagated along the illuminating beam axis, such that the phases of those waves are determined by axial position of scatterers [2]. The axial coherence gating determines the axial speckle sizes, whereas the speckle intensity depends on the number of scatterers within the coherence volume, their scattering strength and their mutual positions. Thus, in OCT speckles are formed by interfrence of multiple waves backstattered from randomly and distributed in space scatterers, random axial positions of which determine random phases of the speckle-forming waves. For interfrence of such multiple waves with uniformly distributed random phases, the statistics of speckle-amplitude in OCT scans should correspond to a Rayleigh distribution [3]. The latter situation is typical of many turbid media with randomly and sufficiently densely located scatters, so that each coherence volume contains multiple scattering centers producing backscattered wave with random phases. For speckle amplitudes with a Rayligh-type statistics, the speckle-contrast pamameter is close to 0.52 (or, equivalently, for speckel intensities the speckle contrast is close to unity) [4]. If scatterers in the tissue are distributed inhomogeneously, e.g., form islands or cell-like structures, this distorts the OCT-speckle statistics, so that the speckle-contrast vaule may be significantly distorted. For example, increased speckle-contrast value may be used to automatically differentiate zones of adipose in OCT images in the context of breast-cancer diagnostics [5]. Thus, assessment of OCT-speckle statistics (in particular, the speckle-contrast parameter) can give valuable diagnostic information about the examined tissues.

However, an important point is that the experimentally observed speckle-contrast in OCT scans may be significantly affected by some other factors that has no direct relation to local characteristics of scatterers for various tissue types which one tries to differentiate using OCT visualization. In particualr, speckle brightness is certainly dependendent on the intensity of the incident and back-propagated optical waves both of which are affected by attenuation of light during the forth-and-back propagation [6,7]. In this context it is important to recall that in OCT the illuminating wavelength is usually chosen within the so-called "transparency windows", so that in real turbid tissues the optical energy loss usually is strongly dominated by optical scattering. Due to these scattering-related losses, for deeper scatterers, as a rule, the illuminating-beam intensity pronouncedly decreases with increasing depth. For OCT scans, this usually leads to a decrease in speckle amplitudes with depth. In some cases, the interplay between the accumulated attenuation and local increase in scattering strength may cause non-monotonic depth dependence of speckle intensities.

Furthermore, variations in local scattering properties may lead to non-local variations in the signal level. For example, for A-scan regions located below localized strong scatterers, the loss of optical-beam energy caused by such increased scattering may lead to appearance of pronounced shadows ("dark tails") below those strong scatterers. An example of such shadows is given in a real structural scan in panel (a) in Fig. 5 (although the entire Fig. 5 will be discussed later in this text). The formation of such shadows due to the optical-beam attenuation leads to the appearance of spatially non-uniform speckle intensity in lateral directions in addition to the axial decrease in speckle intensity caused by the optical energy losses during the forth-and-back propagation. The resultant spatial inhomogeneity of OCT-speckle amplitudes of such origin may be rather pronounced and may strongly distrort the estimated speckle contrast and other statistical speckle properties. However, these scattering-related effects have no relation to local differences in the characterisitcs of scatterers in various morphological components of tissues, the segmentation of which usually is the main goal of OCT-diagnostics.

To eliminate this distorting influence of scattering-related attenuation on the amplitudes and apparent spatial inhomogeneoity of OCT speckles, we propose a refined approach to the analysis of speckle contrast and other parameters characterising local properties of turbid media visualized in OCT scans. The approach is based on depth-resolved compensation of optical attenuation at both local and non-local levels.

In what follows, we will first present some basic equations and demonsrate the efficiency and usefullness of the proposed approach using both simulated OCT signals and real OCT scans.

2. Compensation of optical-attenuation influence on speckle properties in OCT scans

We consider a pixelated two-dimensional OCT B-scan consisting of a number of adjacent one-dimensional axial A-scans. Let us consider a single A-scan in which the uncorrected intensities of pixels along the depth-coordinate z are denoted as $I_0(z_q)$. Recalling that usually in biotissues the attenuation of OCT signals is dominated by scattering, the intensity $I(z_q)$ of q-th pixel in the A-scan after compensation of attenuation can be written as:

$$I(z_q) = \frac{I_0(z_q)}{\exp\left[-2\int_0^{z_q}\mu_s(z)dz\right]} \qquad (1)$$

Here, $\mu_s(z)$ is the scattering-related optical attenuation coefficient (OAC) [6] and the initial intensity in q-th pixel is related to the pixel amplitude $I_0(z_q)=|A_{px}(q)|^2$, where $A_{px}(q)$ is the pixel amplitude.

The optical attenuation coefficient $\mu_s(z)$ in Eq. (1) is yet unknown, so that our aim is to represent Eq. (1) in terms of only directly measured OCT-speckle intensities. Under the assumption of strong domination of scattering in the total optical attenuation, the received-signal intensity can be represented as [6]

$$I_0(z) = J_0\mu_s(z)\cdot\exp[-2\int_0^z\mu_s(z')dz'], \qquad (2)$$

Here, the fist multiplier J_0 is the intensity of the incident illuminating beam. The scattering coefficient $\mu_s(z)$ on the

one hand determines the initial amplitude of the backscattered signal and, on the other hand, integral $2\int_0^z \mu_s(z')dz'$ in the exponential function determines the signal attenuation during its forth-and-back propagation. It should be also pointed out that in Eq. (2) the OCT-signal intensity is affected exclusively by the attenuation. This means that other factors (such as influence of focusing, the fall-off effect typical of spectral-domain OCT and other instrumental factors) are compensated, which can be made, for example, as described in [8].

Now consider an auxiliary integral $\int_z^\infty I_0(z')dz'$. Taking into account Eq.(2) after some transformations one can represent this integral in the following form:

$$\int_z^\infty I_0(z')dz' = \frac{J_0}{2}\exp[-2\int_0^z \mu_s(z')dz'] \qquad (3)$$

Substituting the exponential function from Eq. (3) in Eq. (1), we obtain the sought formula for the corrected pixel intensities $I(z_q)$ expressed via the initially measured intensities $I_0(z_q)$:

$$I(z_q) = J_0 \frac{I_0(z_q)}{2\int_z^\infty I_0(z')dz'} \qquad (4)$$

The ratio $I(z_q)/J_0$ in Eq.(4) coincides with the expression derived in [6] for the spatially-resolved values of the scattering coefficient $\mu_s(z)$ (and equivalently, for the local optical attenuation coefficient under the used assumption of strong domination of scattering in the total attenuation):

$$\frac{I(z_q)}{J_0} = \frac{I_0(z_q)}{2\int_z^\infty I_0(z')dz'} = \mu_s(z) \qquad (5)$$

The obtained Eq. (4) gives the sought corrected expression for pixel intensities in which attenuation-related distortions are eliminated, so that the statistical characteristics of speckles in corrected OCT scans (e.g., the speckle contrast parameter) indeed reflect local properties of scattering turbid medium.

In discrete form corresponding to the pixelated structure of OCT scans, Eq. (4) can be written as:

$$I_q = \frac{1}{2\Delta z_{px}} \frac{I_{0q}}{\left(\sum_{q+1}^{N-1} I_{0j}\right) + \frac{1}{2}\left(I_{0q} + I_{0N}\right)} \qquad (6)$$

where q is the pixel index corresponding to the current depth z_q; Δz_{px} is the axial distance between neighboring pixel centers, and index N corresponds to the maximal depths z_N visualized in the OCT scans.

In what follows, we will demonstrate how the correction of pixel amplitudes affects such a useful and commonly-calculated parameter of speckle images as the normalized speckle contrast parameter defined as [4]:

$$\sigma_I = \frac{\sigma}{\langle I \rangle} = \frac{\sqrt{\langle I^2 \rangle - \langle I \rangle^2}}{\langle I \rangle}, \qquad (7)$$

Here, I is the intensity of OCT signal at each pixel within the processing window used for SC estimation; operator $\langle\ \rangle$ denotes the procedure of pixel-intensity averaging within the chosen processing window; σ is the standard deviation of the intensity within this window. We recall that speckle contrast is expected to tend to unity $\sigma_I \to 1$ for homogeneous scatterer distribution with a high scatterer concentration (with a few and greater number of scatterers in each sample (coherence) volume of the OCT beam) [4]. For small scatterer concentrations (less than unity in each sample volume) or strong spatial inhomogeneities in scatterer distribution in the chosen window, the speckle contrast exhibits spikes $\sigma_I >> 1$. The corresponding examples will be considered in the following sections.

3. OCT speckle pattern simulation with accounting for scattering-dominated attenuation

First, we will demonstrate the influence of the above-described correction procedures using numerically simulated OCT scans. We consider the most widely used case of weakly focused OCT beam enabling approximately axially invariable illuminating-beam diameter. Using the approach [9] to simulating OCT signals, the received complex-valued amplitude $A_{px}(q)$ of q-th pixel in the axially directed one-dimensional A-scan can be found as an inverse Fourier transform of the received spectral components back-scattered from localized point-like scatterers distributed in the simulated tissue:

$$A_{px}(q) = \sum_n \sum_j S(k_n) A_j^{rcv} \exp(i2k_n z_j) \exp(-i\frac{2\pi n}{H} z_q) \qquad (8)$$

Here, A_j^{rcv} is the received amplitude of optical signal back-propagated from each localized (point-like) j-th scatterer; z_q is the depth coordinate corresponding to the center of q-th pixel; n is the index of the discrete spectral components (index n varies from -N/2 to N/2, where we assume that N is an even value and N+1 is the total number of discrete spectral components registered by the receiving array or swept-source system detector); z_j is axial coordinate of j-th scatterer; quantity $k_n = k_0 + \pi n/H$ is the wavenumber of n-th optical-signal component; k_0 is the wave number corresponding to the center wavelength of the broadband light source with the amplitude spectral form $S(k_n)$; H is the maximum imaged depth corresponding to the step $|k_{n+1} - k_n|$ between the spectral components. Good applicability of the simple Eq. (8) to description of OCT-image formation for weakly focused beams was validated by comparison with

more rigorous modeling [10,11] allowing one to accounting for illuminating-beam focusing.

In the initial form of such a model proposed in [9], the received amplitude A_j^{rcv} was assumed to be proportional to the scattering strength of *j*-th scatterer and incident-wave amplitude neglecting the influence of signal attenuation during the forth-and-back propagation. However, actually the optical signal experiences attenuation in equal proportions during the forth- and back-propagation. Recalling that the discussed attenuation is dominated by energy losses due to scattering in the turbid biotissues, one may write for the wave amplitude received from *j*-th scatterer:

$$A_j^{rcv} = \alpha P_j L_j B(x_j, y_j) \qquad (9)$$

Here, α is a coefficient characterising the receiver sensitivity; function $B(x_j, y_j)$ describes the normalized to unity amplitude profile of the considered A-scan at the upper tissue boundary (most commonly this is a Gaussian profile); $L_j \le 1$ is the attenuation coefficient of the intensity of beam propagated from the source to *j*-th scatterer; P_j^2 is the ratio of the beam energy scattered by *j*-th scatterer to the total beam energy at the depth z_j of *j*-th scatterer. This ratio is proportional to the scattering strength of the scatterer; (x_j,y_j) are the lateral coordinates of j-th scatterer.

Assuming that, for the scatterers located within the considered A-scan, indexes *j* are sorted in the direction of increasing depth, and taking into account that the cumulative attenuation L_j is determined by the energy scattering by all previous scatterers when the beam reaches depth z_j, one can write a recurrent formula relating factor L_j at the depth z_j of *j*-th scatterer with factor L_{j-1} describing the cumulative energy loss by depth z_{j-1} and factor P_{j-1} describing the energy scattering by $(j-1)$-th scatterer:

$$L_j = L_{j-1}(1-[B(x_{j-1}, y_{j-1})P_{j-1}]^2) \qquad (10)$$

This recurrent formula holds for indices $j \ge 1$ with the initial values L_0=1 and P_0=0.

Equations (8) in combination with (9) and (10) can be used to simulate OCT scans with accounting for scattering-dominated optical-signal attenuation for arbitrary ensembles of scatterers with coordinates (x_j, y_j, z_j) in the simulated tissue volume. The considered combination of the model Eq. (8) with Eq.(9) and (10) generalizes the initial form of model [9] by accounting the optical energy losses and retaining the usefulness of approach [9] for simulating various OCT modalities.

4. Demonstrations based on numerically simulated and real OCT images

In this section we demonstrate results of OCT-data simulation based on Eqs. (8), (9) and (10) (the model is also deployed at the internet platform OpticElastograph [12]). The first simulated dataset in Fig. 1 shows simulated B-scans for various attenuation levels determined by various scattering strengths of scattering particles. Panels (a-1)-(a-4) represent structural OCT scans with in average homogeneously distributed 257000 scatterers for the simulated-scan size 256 axially and 512 pixels laterally. Panel (a-1) corresponds to the backscattering ratio P_j=0.25%, whereas panels (a-2)-(a-4) are for P_j = 0.5%, 0.75% and 1% , respectively. In terms of energy, scattering/attenuation parameter μ_s used in Eq. (2), the value of μ_s for panel (a-2) is 4 times greater and for (a-4) is 16 times greater than for (a-1).

Panel (b) shows the speckle-contrast parameter (SC) estimated via Eq. (7) for panels (a-1)-(a-4) using different axial sizes of the processing window with a fixed horizontal size equal to the horizontal scan size.

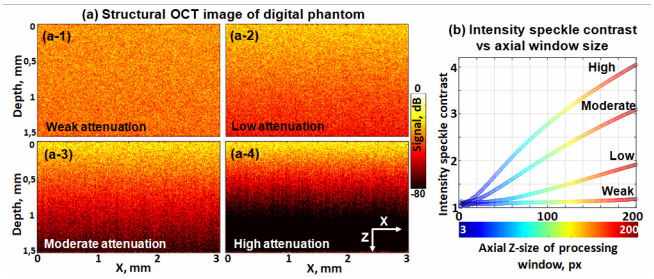

Figure 1. Demonstration of speckle-contrast dependence on optical attenuation due to backscattering in the sample. Panel (a) demonstrates structural OCT scans with various degree on optical attenuation where *P*j are 0.25%, 0.5%, 0.75% and 1% for (a-1) - (a-4) respectively. Panel (b) represents the dependence of intensity speckle contrast on window size for these four cases. For better impression, the window size is also marked by the color of symbols according to the color bar below the graph.

It is evident from Fig. 1b that only for the most weak attenuation the speckle-contrast parameter remains invariable and close to unity value expected for scattering by uniformly and sufficiently densely distributed scatterers with similar scattering strength parameters (i.e. in the absence of very weak and very strong scattering particles). For higher attenuation, the speckle contrast parameter monotonically increases with increased axial size of the processing window. We recall that in all four cases, the speckles were formed by homogeneously distributed similar scatterers, for which SC→1 should be expected. The pronouncedly elevated SC demonstrated in Fig 1b for larger window sizes are caused by the distorting influence of attenuation. The strongest deviation from SC=1 occurs for the strongest attenuation, for which the directly estimated SC-value does not reflect the local properties of scatterers.

To mitigate the distorting effects of attenuation and reconstruct the attenuation-free SC value, the attenuation can be compensated using Eq. (4) or rather by its discretized form, Eq. (6). Figure 2 demonstrates the result of OAC compensation for the OCT scan with the strongest attenuation shown in Fig 1(a-4), according to which one

should expect the maximal influence of the signal attenuation on the estimated SC. The speckle-contrast in Fig. 2 is estimated using windows of two sizes, 10x10 pixels and 30x30 pixels. It is clear that for the initial structural OCT image, the influence of attenuation-induced inhomogeneity leads to artefactual increase in the SC values, especially for a larger processing window (see Figs. 2(a-2) and 2(a-3)). In contrast, for the scan shown in Fig. 2(b-1) obtained from Fig. 2(a-1) using Eq. (6), the SC maps in Figs. 2(b-2) and 2(b-3) demonstrate SC values rather close to the expected unity value.

.

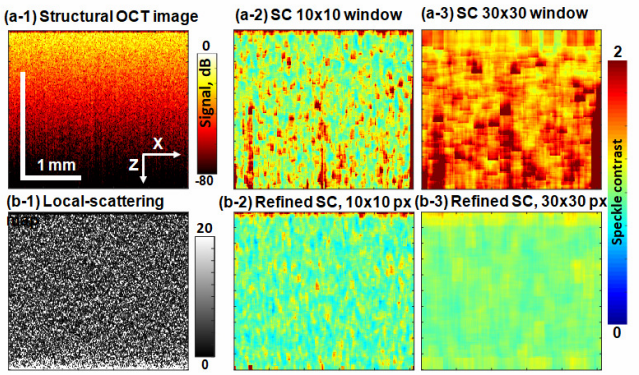

Figure 2. Demonstration of the efficiency of the refined speckle contrast evaluation through attenuation compensation using OCT digital phantom: (a-1) simulated OCT scan for the same as in Fig. 1(a-4) spatially homogeneous distribution of scatterers; (a-2) SC map for 10x10 processing window demonstrating rather noisy values in the range from ~0.8 to ~1.5; (a-3) SC map for 30x30 px processing window demonstrating also noisy and additionally biased (elevated) values because of the stronger influence of optical signal attenuation within the larger processing-window size; (b-1) spatial map of local scattering obtained from the initial scan (a-1) using the attenuation compensation by Eq. (4); (b-2) and (b-3) SC maps for 10x10 pixels and 30x30 pixels processing windows demonstrating restoration of the SC values tending to the expected unutiy value obtained form the restored scattering intensity map (b-1).

The next example in Fig. 3 demonstrates how the apparent speckle contrast may be distorted by the non-local artefacts – the appearance of shadow below localized scatterers with strongly increased scattering strength. The structural image in Fig. 3(a-1) is obtained for the same distribution of scatterers as in Fig. 2(a-1) with a hundred of additional stronger scatterers with pronouncedly increased scattering parameter P_j in comparison to the other scatterers in the phantom bulk. The presence of these scatterers causes the appearance of vertical elongated shadows clearly visible in Fig. 3(a-1). In comparison with Fig. 2, it is clear that the apperance of lateral heterogeneity in addition to the attenuation in the axial direction causes additional strong distortion/bias in the SC maps directly reconstraucted from the initial structural image (Fig. 3(a-2) for 10x10 px window and Fig. 3(a-3) for 30x30 px processing window). Figure 3(b-1) shows the corrected scattering-intensity map obtained from Fig. 3(a-1) using Eq. (4). Figures 3(b-2) and 3(b-3) show the refined speckle-contrast maps obtained from the corrected scattering-intencity scan Fig. 3(b-1) using processing windows 10x10 pixels and 30x30 pixels, respectively. It is clear that such refined SC maps are essentially cleared from the distortions caused by both axial and lateral inhomogeneity of intensity in the initial structural image shown in Fig. 3(a-1), so that the SC value tends to the unity value expected for densely and homogeneously distributed scatterers over the imaged area. The the speckle-amplitude histogram in the inset in Fig. 3(a-1) exhibits a form pronouncedly deviated from a Rayleigh distrubution due to the influence of in-depth attenuation and lateral inhomogeneity caused by shadows. For the corrected scattering-intensity map in Fig. 3(b-1), the similar histogram has a form quite close to the expected Rayleigh distribution of speckle amplitudes.

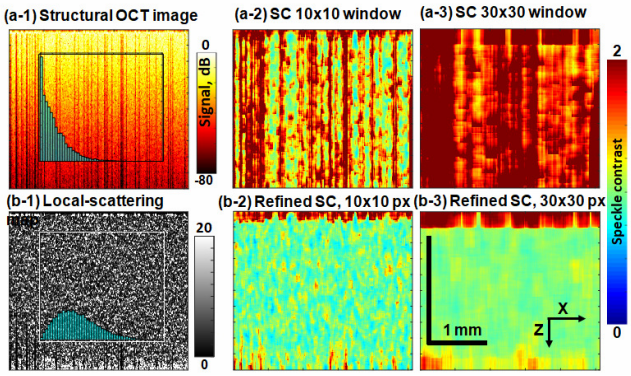

Figure 3. Demonstration of the efficiency of the refined speckle contrast evaluation in the presence of axial signal decay and pronounced lateral inhomogeneity caused by shadows produced by strong near-surface scatterers. (a-1) is the simulated OCT scan with for the same positions/parameters of scatterers as in Fig. 2(a-1) with additional lateral inhomogeneity due to the presence of shadows induced by randomly located strong scatterers near the surface; (a-2) SC map for OCT-image (a-1) for the processing window 10x10 pixels demonstrating very noisy values; (a-3) SC map for OCT-image (a-1) with the processing window 30x30 pixels demonstrating noisy values additionally biased to values >1 because of the combined influence of regular attenuation in the axial direction and lateral inhomogeneity caused by the shadows; (b-1) corrected scattering-intensity map obtained from (a-1) using Eq. (4); (b-2) refined SC map for the corrected scattering-intensity map (b-1) and processing window 10x10 pixels; (b-3) refined SC map similar to (b-2) for processing window 30x30 pixels. Insets in (a-1) and (b-1) show amplitude histograms found within rectangles covering the entire scan width of 512 px laterally and 30 px axially.

The examples shown in Figs. 2 and 3 demonstrate the efficiency of the proposed procedure of obtaining corrected scattering-intensity maps starting from the OCT scans in which the apparent scattering intensity is essentially distorted. This distortion is caused by the influence of scattering-induced attenuation in the depth direction, as well as by lateral inhomogeneity caused by formation of shadows below strong scatterers which may occur is the sample. For the corrected images (like in Fig. 2(b-1) and 3(b-1)), the refined spackle-contrast maps are essentially cleaned form the above-mentioned distorting effects and much clearer

reflect the local properties of distribution of scatterers in the imaged tissue.

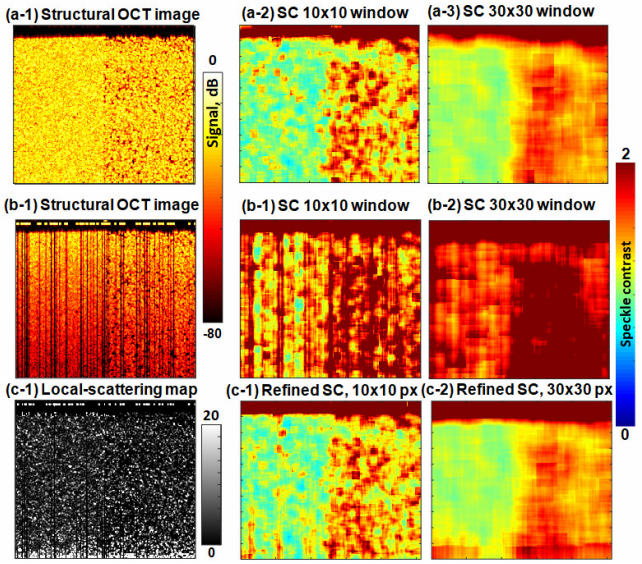

Figure 4. Demonstration of the efficiency of the refined speckle contrast evaluation through attenuation compensation for simulated OCT scans with homoheneous distribution of scatterers in the left half of the OCT scans and spatially-inhomogeneous pattern (with "holes") in the right half of the scan. (a-1) is the OCT scan simulated for extremely weak signal attenuation, so that the visible scattering intensity in the OCT image is entirely determined by the local distribution and strength of scatterers; (a-2) and (a-3) are the SC-maps obtained for the OCT scan in panel (a-1) with a clear difference between the left and right halves in terms of the SC-value; (b-1) is simulated similarly to (a-1) additionally taking into account scattering-induced in-depth optical attenuation and apperance of lateral inhomogeneity due to formation of shadows below strong near-surface scattterers; (b-2) and (b-3) are the SC maps obtained for scan (b-1) demonstrating that the difference in SC-values between the left and right scan halves is strongly corrupted by the scattering-related effects; (c-1) is the corrected scattering-intensity map obtained from (b-1) using Eq. (4); (c-2) and (c-3) are refined SC map for 10x10 px and 30x30 px processing windows, respectively, demonstrating the restored difference between the left and right halves of the scan in terms of SC-value.

We recall the estimation of speckle-contrast parameter may be efficiently used, for example, for differentiating other tissue components from adipose tissue during OCT examination of breast cancer tissues [5]. Adipose exhibits peculiar spatially-inhomogeneous distribution of scatterers forming specific cellular patterns in OCT images, so that this tissue component may be segmented using the increased SC-value in adipose zones. Figures 4(a-1)-(a-3) demonstrate a simulated situation characterized by such a difference in the distribution of scatterers. Namely, the structural scan in Fig 4(a-1) is simulated using Eq. (8) in the limit of very weak signal attenuation. In the left part of Fig. 4(a-1) the scatterers are distributed fairly homogeneously (which is typical of the majority of tissue components) and in the right-hand part of the scan, the scatterer distribution exhibits an inhomogeneous patters resembling cellular pattern typical of adipose tissue. Correspondingly, the SC maps in Figs. 4(a-2) and 4(a-3) clearly demonstrate an increased SC-value, which may be used to efficiently automatically segment the left and right halves of such a tissue components.

However, real structural scans are usually affected by pronounced scattering-related OCT-signal attenuation as demonstrated in Fig 4(b-1). The latter is simulated for the same distribution of scatterers in the tissue bulk but with a number of fairly strong scatterers at the tissue surface (producing some shadow), as well as by taking into account OCT-signal attenuation (by putting the scattering parameter P_j=1% similarly to Figs. 2(a-1) and 3(a-1). The SC maps shown in Fig. 4(b-2) and (b-3) that are directly calculated for the structural scan in Fig. 4(b-1) demonstrate that in terms of SC parameter the difference between the left and right halves of the OCT scan is strongly masked.

Next, Fig. 4(c-1) shows the corrected map of scattering-intensity obtained from Fig. 4(b-1) using Eq. (4). In the corrected map the difference between the left and right parts of the scans becomes cleared from the scattering-related distortions. Correspondingly, the maps of refined estimation of SC parameter in Fig 4(c-2) and 4(c-3) demonstrate that in terms of the SC-value the difference between the left and right parts of the OCT scan again becomes well visible much like for the SC-maps in Figs. 4(a-2) and 4(a-3).

Finally, in addition to simulated scans we demonstrate the refined speckle contrast estimation for a real OCT scan of a sample of homogenous silicone, in the OCT scan of which pronounced vertical shadows appear due to the presence of some strongly scattering dust particles on the surface. The structural scan in Fig. 5(a-1) clearly shows such shadows. The corresponding SC map presented in Fig. 5(a-2) demonstrates the appearance of pronounced spikes in the SC-vales in the vicinity of the shadows, although the distribution of scatterers in the silicone bulk is rather homogeneous. After correction of the scattering-related attenuation we obtain the scattering-intensity map with a much more spatially homogeneous intensity of speckles as shown in Fig. 5(b-1), in which the shadows are strongly suppressed. The corresponding refined SC map in Fig. 5(b-2) also demonstrates that the shadowing-related spikes are strongly suppressed and the SC distribution becomes much closer to the unity value as expected for a dense, in average homogeneous distribution of scatterers.

It may be also noted that the upper stripes visible in the speckle-contrast maps in Fig. 5 are related to the vertical size of the processing window used for calculation of the speckle contrast. When the window covers the boundary between the scattering tissue and the upper space with (almost) absent scatterers, the calculated SC-value for such a window gets strongly increased. Correspondingly, for the larger window of 30x30 px in size, the width of the upper stripe is greater in comparison with the maps found for 10x10 px window.

The stripe of the increased SC-value visible near the bottom of Fig. 5(b-3) has another origin. We recall that the corrected map of scattering intensity in Fig. 5(b-1) is found via Eq. (6) corresponding to the estimation of local scattering strength in Vermeer's approach [6]. When this approach is applied to an OCT scan with incomplete decay of the OCT near the bottom, the denominator of discretized Eq. (6) is underestimated in comparison to Eq. (4) written in the continuous form. Correspondingly, the corrected local values of scattering intensity become somewhat overestimated with stronger overestimation closer to the scan bottom, which is a well known feature of Vermeer's approach [13]. This effect is discernible near the bottom in Fig. 5(b-1). In the SC-value map found for the larger 30x30 px window in Fig.5(b-3) lead to the appearance of artefactual stripe of evelated SC-values near the bottom. The near-bottom intensity inhomogeneity in Fig. 5(b-1) is less critical for the smaller processing window 10x10 px and does not lead to the appearance of pronounced stripe of enhanced SC-value in Fig. 5(b-2), in contrast to Fig. 5(b-3),

In comparison with Fig. 5(b-3) for the real example with moderate in-depth attenuation, the near-bottom artefactual stripes of enhanced SC-vales are not so pronounced for the digital phantoms in Figs. 2, 3 and 4 because of stronger attenuation (compare, for example, Fig. 3(b-3) and Fig. 5(b-3)).

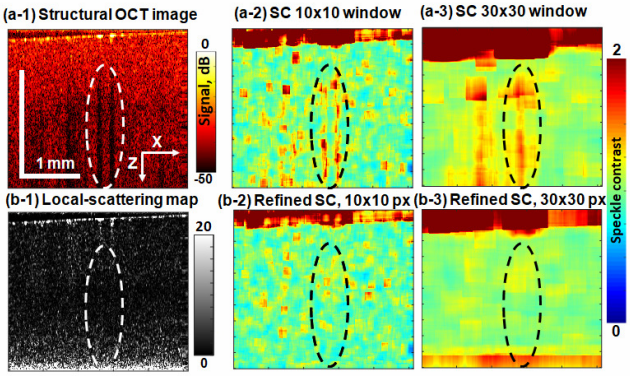

Figure 5. Demonstration of the efficiency of refinied speckle-contrast estimation using real OCT data for a silicone sample with some on-surface bright scatterers producing shadows. (a-1) structural OCT scan; (a-2) SC map obtained for 10x10 px processing window demonstrating distorted noisy values at the areas affected by shadows indicated by dashad ovals; (a-3) is a similar SC-map for 30x30 px window, for which SC-values demonstrate even stronger distortion caused by shadow influence; (b-1) corrected map of scattering-intensity in which the shadows are strongly suppressed; (b-2) and (b-3) are refined SC maps demonstrating the restoration of the SC-value much closer to the expected unity value and obtained for processing-window sizes 10x10 and 30x30 pixels, respectively.

5. Discussion and conclusions

In this study, we present a simple and practically convenient approach to characterization of local scattering properties of tissues via refined speckle contrast estimation in OCT scans. The proposed refined SC parameter is determined by local parameters of scatterers and is not affected by the optical signal gradients caused by scattering-related attenuation. The latter determines the signal decay in the axial direction, as well as the appearance of shadowing effect caused by the presence of localized strong scatterers. This effect may produce pronounced lateral heterogeneity besides the widely discussed signal attenuation in the depth direction as shown in the real OCT scan in Fig. 5(a-1).

The digital phantoms generated in this study to demonstrate the distorting scattering-related effects as well as the efficacy of the compensation procedures are available at repository [14]. For generating such digital phantoms, the previously proposed simple model [9] of OCT-signal formation by a weakly focused illuminating beam (see basic Eq. (8)) was supplemented by Eqs. (9) and (10) allowing one to readily introduce scattering-dominated attenuation of OCT signal. Due to the proposed scattering-compensation procedures, the corrected scattering-intensity maps can be cleared from the distorting influence of the scattering-induced in-depth attenuation, as well as the lateral inhomogeneity caused by shadows below strong scatterers. Correspondingly, the statistical properties of speckles in the corrected maps are determined by genuine local properties of scatterers in the imaged tissue, which is very important for making correct diagnostic conclusions based on analysis of OCT-scans and for the development OCT-modalities beyond conventional structural imaging [15].

Acknowledgements

The study was supported by the RSF Grant No. 23-72-01107 in part of the development of the approach to OCT-signal simulation with accounting for scattering-dominated attenuation and procedures of its compensation. Generation of simulated datasets and numerical testing was supported by the Ajman University grant No 2023-IRG-ENIT-44.

References

[1] Bouma B E, de Boer J F, Huang D, Jang I K, Yonetsu T, Leggett C L, Leitgeb R, Sampson D D, Suter M, Vakoc B J, Villiger M and Wojtkowski M 2022 Optical coherence tomography *Nat. Rev. Methods Prim.* **2**

[2] Fujimoto J G, Brezinski M E, Tearney G J, Boppart S A, Bouma B, Hee M R, Southern J F and Swanson E A 1995 Optical biopsy and imaging using optical coherence tomography *Nat Med* 1 970–2

[3] Schmitt J M, Xiang S H and Yung K M 1999 Speckle in optical coherence tomography. *J. Biomed. Opt.* **4** 95–105

[4] Weatherbee A, Sugita M, Bizheva K, Popov I and Vitkin A 2016 Probability density function formalism for optical coherence tomography signal analysis: a controlled phantom study *Opt. Lett.* **41** 2727

[5] Plekhanov A A, Gubarkova E V, Sirotkina M A, Sovetsky A A, Vorontsov D A, Matveev L A, Kuznetsov S S, Bogomolova A Y,

Vorontsov A Y, Matveyev A L, Gamayunov S V, Zagaynova E V, Zaitsev V Y and Gladkova N D 2023 Compression OCT-elastography combined with speckle-contrast analysis as an approach to the morphological assessment of breast cancer tissue *Biomed. Opt. Express* **14** 3037

[6] Vermeer K A, Mo J, Weda J J A, Lemij H G and De Boer J F 2014 Depth-resolved model-based reconstruction of attenuation coefficients in optical coherence tomography *Biomed. Opt. Express* **5** 322

[7] Gong P, Almasian M, Van Soest G, De Bruin D M, Van Leeuwen T G, Sampson D D and Faber D J 2020 Parametric imaging of attenuation by optical coherence tomography: review of models, methods, and clinical translation *J. Biomed. Opt.* **25** 1

[8] Sovetsky A A, Matveyev A L, Matveev L A, Chizhov P A and Zaitsev V Y 2024 Simple “Digital Phantom” for Testing Attenuation-Imaging Methods in Optical Coherence Tomography *J. Biomed. Photonics & Engineering* **10** 020302

[9] Zaitsev V Y, Matveev L A, Matveyev A L, Gelikonov G V and Gelikonov V M 2014 A model for simulating speckle-pattern evolution based on close to reality procedures used in spectral-domain OCT *Laser Phys. Lett.* **11** 105601

[10] Matveyev A L, Matveev L A, Moiseev A A, Sovetsky A A, Gelikonov G V and Zaitsev V Y 2019 Semi-analytical full-wave model for simulations of scans in optical coherence tomography with accounting for beam focusing and the motion of scatterers *Laser Phys. Lett.* **16** 085601

[11] Matveyev A L et al 2024 K-Space Approach in Optical Coherence Tomography: Rigorous Digital Transformation of Arbitrary-Shape Beams, Aberration Elimination and Super-Refocusing beyond Conventional Phase Correction Procedures *Sensors* **24** 2931

[12] https://www.opticelastograph.com/

[13] Liu J, Ding N, Yu Y, Yuan X, Luo S, Luan J, Zhao Y, Wang Y and Ma Z 2019 Optimized depth-resolved estimation to measure optical attenuation coefficients from optical coherence tomography and its application in cerebral damage determination J. Biomed. Opt. 24(3) 035002

[14] https://github.com/OCTDigitalPhantoms

[15] Leitgeb R, Placzek F, Rank E, Krainz L, Haindl R, Li Q, Liu M, Andreana M, Unterhuber A, Schmoll T and Drexler W 2021 Enhanced medical diagnosis for dOCTors: a perspective of optical coherence tomography J. Biomed. Opt. 26 100601